Modelling of ICRH in a Tokamak including Large Banana Width Effects

L-G Eriksson, J Carlsson[1], T Hellsten[1].

JET Joint Undertaking, Abingdon, Oxfordshire, OX14 3EA, UK.
[1] Royal Institute of Technology, S-10044 Stockholm, Sweden.

Abstract Modelling of ICRH in a Tokamak, with special emphasis on finite banana width effects, is discussed. Comparison between simplified modelling and experimental results is used to illustrate the importance of finite orbit width effects. These effects can be modelled more rigorously with an orbit averaged Fokker-Planck equation, its derivation and solution by a Monte Carlo method is outlined. Results from a code solving the equation along these lines are presented.

1. INTRODUCTION

Ion Cyclotron Resonance Heating (ICRH) has proved to be a successful method for auxiliary heating of Tokamaks. In JET it is one of the main heating methods with a potential of coupling about 25 MW of RF-power into the plasma [1]. There are several advantages with ICRH: the fast magnetosonic wave, which carries the ICRH power, can penetrate and deposit the power efficiently at the centre of large dense plasmas; the power deposition profile can be tailored to some extent by moving the cyclotron resonance, which can be utilised for minority current drive aimed at sawtooth stabilisation [2]; the generation of the RF-power is based on well established technology. The ability of ICRH to deposit power efficiently at the centre of large dense plasmas makes it a reactor relevant method for auxiliary heating. In view of this, it is important to understand and model ICRH physics. Modelling of ICRH is quite complicated. There are two main processes that have to be considered, viz., propagation and absorption of the launched waves and the evolution of the velocity distribution(s) of the resonating ions. As an added complication, the wave propagation and the velocity distribution(s) depends on each other, making self-consistent calculations necessary. Another complicating factor is the orbit topology of fast ICRH accelerated ions, especially the finite width of trapped banana orbits. In recent years it has become apparent that it is important to include the finite orbit width in simulations of ICRH [3,4,5]. In this paper ICRH modelling, with special emphasis on the inclusion of finite banana width effects, is discussed.

Comparisons between experimental results and simulations of ICRH are of importance, particularly for assessing the accuracy of the modelling and for identifying areas where improvement is needed. In order to facilitate comparisons with experimental results a code, named PION-T, was developed. It is based on simplified models, making it relatively fast and suitable for routine analysis of discharges. The code calculates the time evolution of the power deposition and the velocity distribution of the resonating ions. Furthermore, the velocity distribution is taken into account in the power deposition model. A short description of the PION-T code together with a brief review of comparisons between experimental results and simulations are given in Section 2. Good agreement between experimental results and the POIN-T simulations is found when the characteristic power densities are low to moderate. However, for high power densities and low concentrations of resonating ions clear discrepancies are observed. These discrepancies are believed to be caused by finite banana width effects. The importance of such effects can be understood if one considers that the resonating ions in JET often are accelerated up to energies in the MeV range. Fig. 1 shows a trapped 1 MeV hydrogen orbit with a turning point close to the centre of the plasma, such an orbit is typical for ICRH accelerated ions in JET. As can be seen, the orbit is shaped like a potato rather than a banana. The typical width of potato orbits, δ_p, is given by [6]: $\delta_p = \Delta^{2/3}R$, where $\Delta = 2q\rho/R$, q is the safety factor, ρ is the Larmor radius and R is the major radius. For the orbit shown in Fig. 1 the width, with typical JET parameters (R = 3m, B_0 = 3T, q = 1, is about 30 cm, i.e. a significant fraction of the plasma radius. In order to do a more quantitative assessment of the importance of finite orbit width effects, a simplified model for taking the finite banana width into account was implemented in modified version of the code, PION-TO. With PION-TO one obtains good agreement also for cases with high power densities. From this and other related studies [3,4,5] it is clear that a rigorous treatment of the effect of finite orbit width on the evolution of the distribution function of ions accelerated by ICRH is needed.

The model used in PION-TO takes into account the enhanced slowing down experienced by energetic ions as a result of their orbits reaching out to the colder parts of the plasma. However, in an accurate modelling of the energetic ions it is not enough to take this effect into account. One must, in addition, include neo-classical transport and RF-induced spatial diffusion, both have been shown to be of importance for describing the energetic ions [7,8]. The evolution of the distribution function of the resonating ions, including the effects due to large banana width, can be described by a three dimensional orbit averaged Fokker-Planck equation. The derivation of the orbit averaged Fokker-Planck equation and its solution by a Monte Carlo method is outlined here. Furthermore, results from the Monte Carlo code FIDO, which solves the orbit averaged Fokker-Planck equation along the lines given in this paper, are presented.

2. SIMULATIONS WITH THE PION-CODE

The PION-T code calculates the time evolution of the ICRH power deposition and the velocity distribution(s) of resonating ions. In the power deposition calculation deviations from a Maxwellian velocity distribution are taken into account.

The power deposition is modelled by a formula described by Hellsten and Villard [9], and further developed by Hellsten and Eriksson [10]. The model is heuristic and was obtained by analysing results from the toroidal full wave code LION [11]. The formula expresses the flux surface averaged Poynting flux for a single mode in a toroidal Fourier expansion as sum of two flux surface averaged Poynting fluxes. One representing single pass, or strong, absorption, $P_1(s)$, and the second representing weak absorption, $P_2(s)$

$$P(s) = \kappa P_1(s) + (1 - \kappa)P_2(s)$$

where s is the flux surface label, $\kappa = a^2\,(2 - a)$, and a is the single pass absorption coefficient across the midplane. The functions P_1 and P_2 are composed of contributions from ion cyclotron absorption by resonating ions and direct electron absorption via electron Landau damping and transit time magnetic pumping (TTMP). The contribution from a resonating ion species, P_{1i}, to P_1 depends mainly on the Doppler broadening of the cyclotron resonance, i.e. on the toroidal mode number, N, and the averaged square parallel velocity, $< v_{\|i}^2 >$ of the resonating species; whereas the contribution P_{2i}, to P_2 depends on the absorption strength and averaged electric field along the cyclotron resonance. The normalised averaged electric field is a calibration function which has been obtained from analysis with the LION code. It turns out to be rather insensitive to specific equilibria and scenarios. In order to make the code fast, the absorption coefficients needed in the model are calculated using the WKB approximation. However, more accurate calculations can in principle be used. For further details about the power deposition model the reader is referred to Refs. [5,9,10].

In order to reduce the computing time the full 2D velocity distribution is not calculated. Instead, the pitch angle averaged velocity distribution is calculated together with a model for obtaining the averaged square parallel velocity of the resonating ions. The evolution of the pitch angle averaged velocity distribution is described by the following Fokker-Planck equation [12]

$$\frac{\partial F}{\partial t} = \frac{1}{v^2}\frac{\partial}{\partial v}\left\{\left[-\alpha v^2 + \frac{1}{2}\frac{\partial}{\partial v}\left(\beta v^2\right)\right]F + \frac{1}{2}\beta v^2\frac{\partial F}{\partial v}\right\} + \frac{1}{v^2}\frac{\partial}{\partial v}\left[v^2 D_{RF}(v)\frac{\partial F}{\partial v}\right]$$

$$D_{RF} = K|E_+|^2\int_{-1}^{1}\left|J_{n-1}\left(k_\perp v\sqrt{1-\mu^2/\omega_{ci}}\right) + \frac{E_-}{E_+}J_{n+1}\left(k_\perp v\sqrt{1-\mu^2}/\omega_{ci}\right)\right|^2 d\mu$$

where the collision coefficients, α and β can be found in Ref. [13], K is a constant related to the absorbed power density, E_+ and E_- are the left and right hand components of the electric field, respectively.

The averaged squared parallel velocity is obtained from the following formula

$$< v_{\|}^2 >= \int_0^{\infty} \mu_{eff}^2(v) F(v) 4\pi v^2 dv, \qquad \mu_{eff}^2 = \frac{1}{3}\left[1+\left(\frac{v}{v_*}\right)^2\right] \Big/ \left[1+\left(\frac{v}{v_*}\right)^2+\left(\frac{v}{v_*}\right)^4\right]$$

where $v_* \sim v_\gamma$, v_γ is the characteristic velocity associated with pitch angle scattering [13]. The above models have been benchmarked against the 2D code BAFIC [12,14] and found to be in satisfactory agreement.

Finite banana width affects are included in a simplified way in a version of the code called PION-TO. In this version the fast ions are assumed to be trapped with their turning points close to the cyclotron resonance. The collision coefficients α and β are then averaged, for each velocity, over the fast ion orbit. In the calculation of profile quantities, like the fast ion pressure and the collisional power transfer to the background plasma, the finite banana width is also taken into account.

The velocity distribution influences the power deposition in mainly two ways: (i) the parallel component affects the Doppler broadening of the cyclotron resonance and to some extent the absorption strength (ii) the perpendicular component affects mainly the absorption strength. From the Fokker-Planck calculations one can calculate the enhancement in absorption strength, $\gamma_\alpha = p_\alpha / p_\alpha^M$ caused by the presence of a high energy tail, where p_α is the power density absorbed the actual distribution and p_α^M is the power absorbed by a Maxwellian distribution with the same density. For the calculation of the absorption coefficients in the power deposition model an absorption strength corresponding to a Maxwellian distribution enhanced by a factor γ_α is used, making the absorption strength in the power deposition model consistent with the Fokker-Planck calculation. The flow chart of the PION-T code is shown in Fig. 2.

Comparison between experimental results and simulations with the PION-T code have been carried out [5]. A few of the results will be reproduced here. Fig. 3 shows a comparison between the measured and calculated perpendicular fast ion energy content (the measured one is obtained by taking the difference between two different measurements of the plasma energy which put different weights on the parallel and perpendicular components [5]) for JET discharge #19650. The heating scenario was hydrogen minority heating in deuterium and was characterised by the following parameters: T_e = 9keV, T_i = 6.5keV, $n_e = 5 10^{19}$ m^{-3}, f = 48MHz, B_0 = 3.1T, P_{RF} = 9.5MW. In this discharge the power density was fairly low because the resonance was off-axis and the power level moderate.

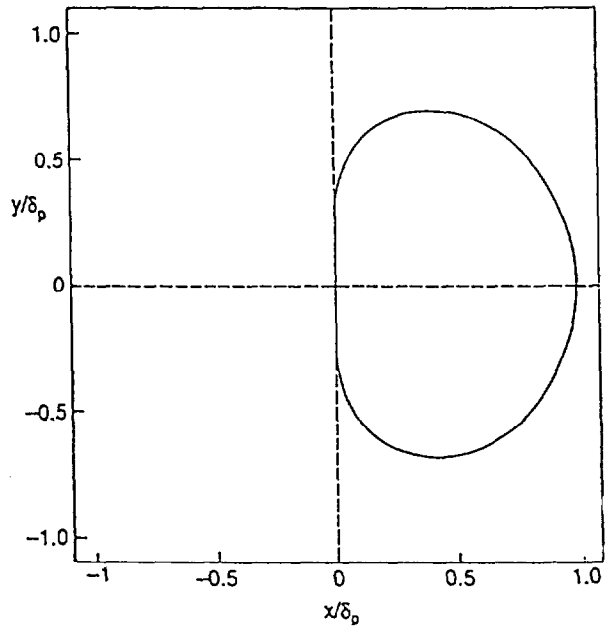

Fig. 1 1 MeV trapped hydrogen orbit with its turning point on the magnetic axis, for typical JET parameters (R = 3m, B = 3T, q_o = 1) $\delta_p \approx 30$ cm.

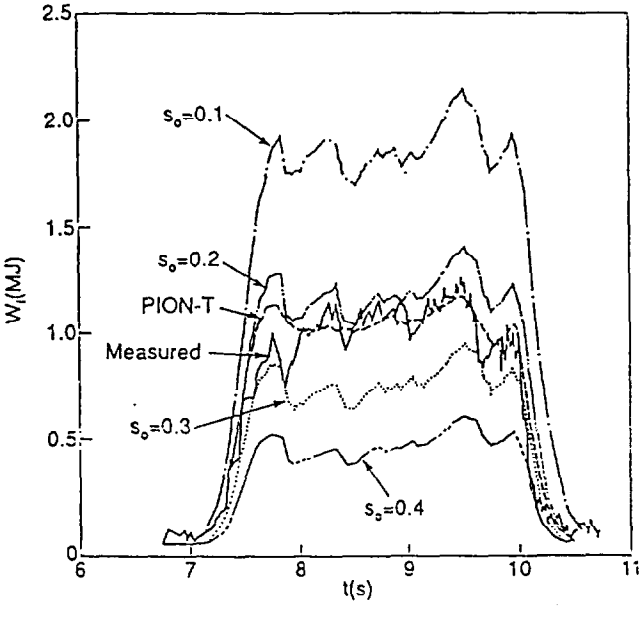

Fig. 3 Anisotropic fast ion energy content of discharge #19650 measured and calculated by PION-T. The curves labelled by s_o = 0.1, 0.2, 0.3 and 0.4 are for the Gaussian power deposition profile with s_o being the half width.

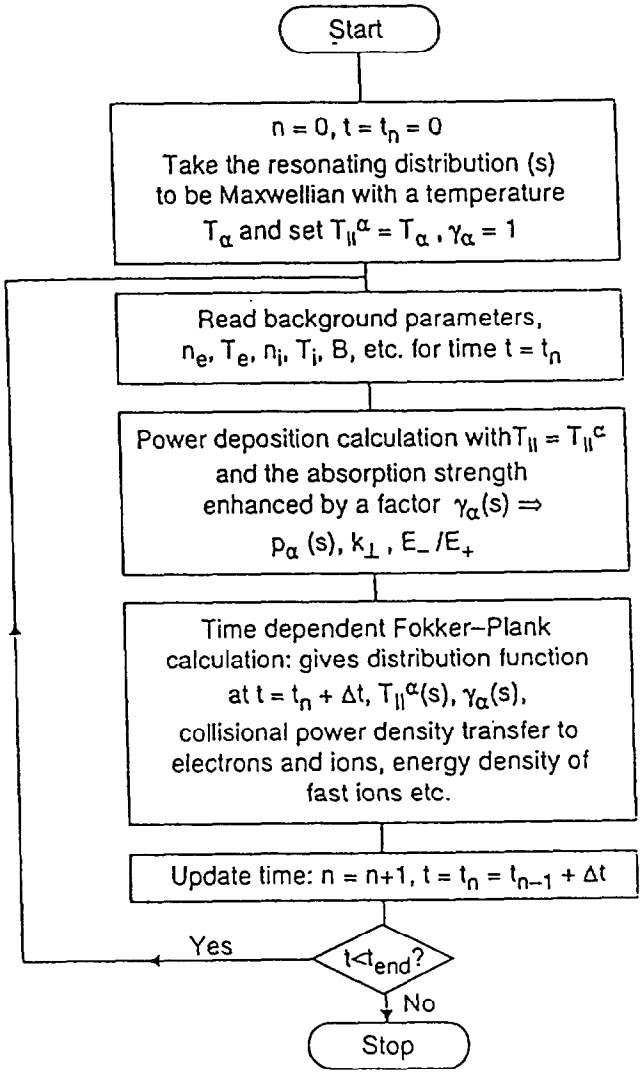

Fig. 2 Flow chart of the PION-T code.

Large banana width effects should therefore not play a major role. As can be seen in Fig. 3 the PION-T code reproduces the measured fast ion energy content quite well. In order to investigate the sensitivity of the results with respect to the width of the power deposition profile, a simple power deposition model with a Guassian shape and variable width has been used. The result of calculations with this model deposition are also shown in Fig. 3. The simulations show that the fast ion energy content is quite sensitive to the width of the power deposition. It is not possible to reproduce the experimental results unless the width of the deposition is close to the one calculated with the PION-T code. This and similar simulations of other discharges give support for classical slowing down of the ions. Furthermore, they indicate that the peaked deposition profiles predicted by power deposition codes are consistent with experimental results. However, for discharges where the absorbed power densities are large and the slowing down times are long, which is the case for most high power ICRH discharges in JET, discrepancies between simulations and experiments appear. Fig. 4 shows a comparison between simulations and measurements of the fast ion energy content for two JET discharges, #12295 and #12298. Discharge #12295 had an RF-power of 4.5 MW whereas #12298 had 8 MW. The cyclotron resonance was close to the magnetic axis for both discharges, which resulted in high power densities for discharge #12298.

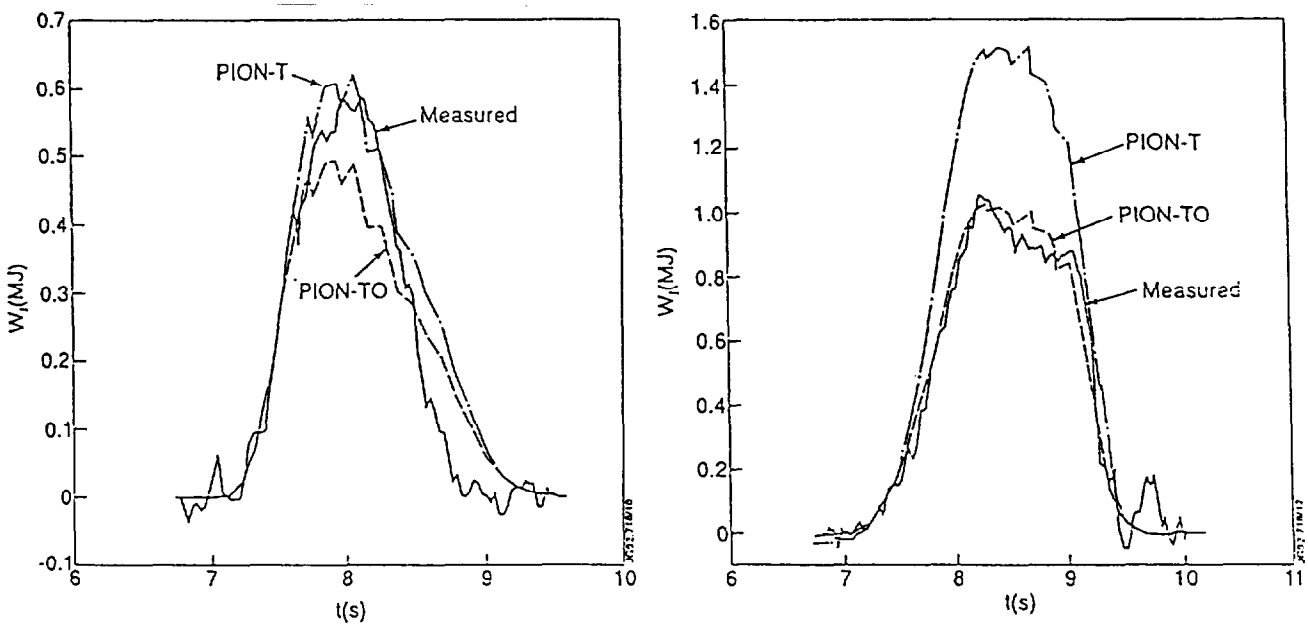

Fig. 4 Anisotropic fast ion energy content measured and calculated (the calculations with PION-TO includes finite orbit width effects),
(a) discharge #12295,
(b) discharge #12298.

The PION-T code, without taking large banana width into account, can reproduce the fast ion energy content of #12295 but severely overestimates it for #12298. However, by using the PION-TO version of the code which takes the finite width of the banana orbit into account, the experimental results for #12298 can be reproduced as well. The conclusion one can draw from these simulations is that the proper inclusion of large banana width effects in the Fokker-Planck calculations is an important problem to address.

3. FOKKER-PLANCK TREATMENT INCLUDING LARGE BANANA WIDTH EFFECTS

There will be an effect on both the distribution function of the resonating ions and the dielectric properties of the plasma when finite orbit width effects are taken into account. The latter being indirectly affected via the distribution function. Here, however, the discussion will be limited to how finite orbit width effects can be included more rigorously in Fokker-Planck calculations of distribution functions.

The purpose of paragraphs 3.2 and 3.3 is to give an outline of the derivation of the orbit averaged Fokker-Planck equation and its solution by a Monte Carlo method. However, many details, which can be found in Refs. [15], have been left out. A derivation of the orbit averaged Fokker-Planck equation involving only the collision operator together with calculations of neo-classical ion fluxes can also be found in ref. [16].

Results from the Monte Carlo code FIDO are presented in paragraph 3.4. However, before turning to the orbit averaged Fokker-Planck equation it is worthwhile to briefly discuss orbits of high energy ions.

3.1 High energy ion orbits

As can be seen in Fig.1, the effect of increased energy on a trapped ion orbit is not just to make the banana width larger. In the regime $\delta_b \geq r$, where $\delta_b \sim \varepsilon^{1/2} q\rho$ is the standard banana width; $\varepsilon = r/R$; q is the safety factor and ρ is the Larmor radius, the banana-shaped orbit is distorted into a potato shaped orbit. The characteristic width, δ_p, of the potato orbit is given by [6]: $\delta_b = \Delta^{2/3} R$, $\Delta = 2q\rho/R$.

Since a significant fraction of fast ICRH accelerated ions in JET often enters the regime $\delta_p \geq r$, information about the orbit topology of such ions is important for calculations of their distribution function. The topology turns out to be quite complicated and is beyond the scope of this paper. Detailed accounts can be found in Refs. [6,17,18]. It is, however, instructive to consider a few examples of non-standard orbits.

One can use three invariants of the motion to identify an orbit (and to find the orbit equation), e.g. the energy $E = \frac{1}{2}mv^2$, the magnetic moment $\mu = mv_\perp^2 / (2B)$ and the toroidal angular momentum $P_\phi = Ze\psi - mRv_{||} B_\phi/B$, where ψ is the poloidal flux. Figs. 1, 5 and 6

shows orbits for three different triplets of E, μ, P_ϕ. For simplicity the orbits shown here are assumed to be confined to an area with low shear i.e. $q \simeq$ const. Furthermore, the axis have been normalised to the potato width δ_p, which for a 1 MeV hydrogen orbit and typical JET parameters (R = 3m, B_0 = 3T, q_0 = 1) is: δ_p = 30 cm.

The orbit shown in Fig. 1 has $E/\mu B_0 - 1 = 0$ and $P_\phi = 0$ ($\psi = 0$ at the magnetic axis). It is typical for ions absorbing power near the magnetic axis. In Fig. 5 two orbits given by $(E/\mu B_0 - 1)R/\delta_p = 0.92$, $P_\phi 2q/(ZeB_0\delta_p^2) = 0.93$ are shown. The outer orbit is mirror trapped whereas the inner orbit is counter passing on the high field side. Finally Fig. 6 shows a trapped orbit with the inner leg on the high field side given by $(E/\mu B_0 - 1)\, R/\delta_p = 0.85$, $P_\phi 2q/(Z_e B_0 \delta_p^2) = 0.9$.

In addition to the orbit types shown here several other exists. In Ref. [6], using some simplifications, eight topologically different regions in invariant space has been found. Thus, the problem of treating high energy ions properly is more complicated than just taking the finite width of banana orbits into account.

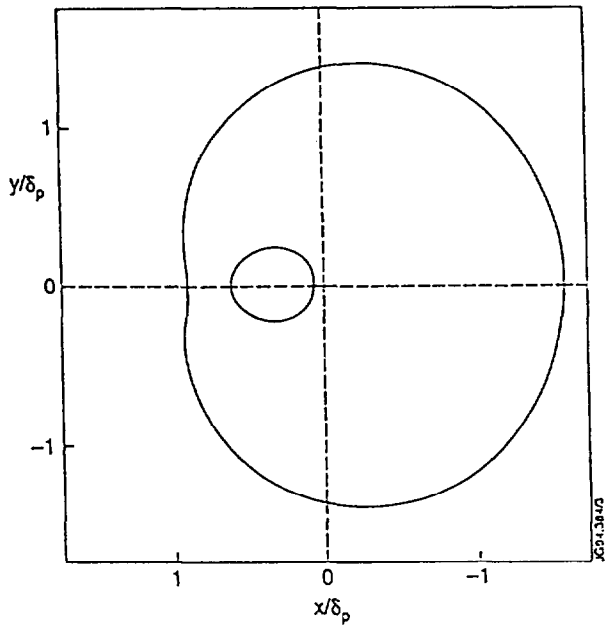

Fig. 5 Two orbits belonging to the same triplet of E, μ, P_ϕ, the outer orbit is mirror trapped and the inner one is counter passing.

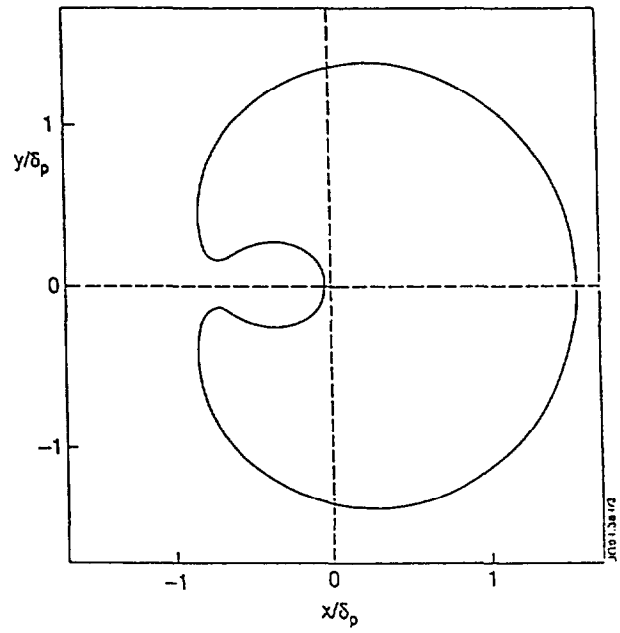

Fig. 6 Fat banana orbit encircling the axis.

3.2 The Orbit Averaged Fokker-Planck Equation

The kinetic equation describing the distribution function can be written as

$$\frac{\partial f}{\partial t} + \dot{z}^i \frac{\partial f}{\partial z^i} = C(f) + Q(f)$$

where C(f) is the collision operator, Q(f) is the operator describing wave particle interaction and z^i are arbitary phase-space coordinates (summation over repeated indices is understood throughout this paper).

In a hot tokamak, the time scales for collisions and wave particle interaction are in general large in comparison with the time it takes for an ion to complete an orbit, τ_b (the bounce time). An expansion of the distribution function, $f = f_0 + f_1 + ...$, in τ_b/τ_s is therefore advantageous, where τ_s is the slowing down time, i.e. the characteristic time for the collisions. In the following only the behaviour of f on the longer timescale, i.e. the evolution of f_0 will be considered.

The unperturbed motion of a particle in an axisymmetric tokamak may be described by action angle variables $(\vec{J},\vec{\theta})$ [15], such that the unperturbed Hamiltonian, H_0, depends on the action angle variables only, $H_0 = H_0(\vec{J})$, and the angles evolves linearly in time, $\dot{\theta} = \partial H_0 / \partial J^i$. Roughly speaking, θ^1 describes the position in the Larmor rotation, θ^2 the position along the guiding-centre orbit, and θ^3 the toroidal position of the banana centre. The orbit averaged Fokker-Planck equation describing the evolution of f_0 is obtained by averaging the kinetic equation over these angles [15], the result is

$$\frac{\partial f_o}{\partial t} = < C(f_o) + Q(f_o) >$$

where $f_o = f_o(\vec{J},t) = < f >$. Due to axisymmetry and the smallness of the Larmor radius, the integrations over θ^1 and θ^3 are trivial and the averaging simply amount to

$$< \cdots > = \frac{1}{2\pi} \int_0^{2\pi} (...) d\theta^2 = \frac{1}{\tau_b} \int_0^{\tau_b} (...) d\tau$$

where τ is the time along the orbit.

At this point it is not necessary to use the action angle invariants and one can change coordinates to some other, more convenient, set of invariants $\vec{I} = \vec{I}(\vec{J})$.

The local collision operator conserves particles and can therefore be written as a divergence. In the coordinates $x^i = (\vec{I},\vec{\theta})$ one has

$$C(f) = g^{-1/2} \frac{\partial}{\partial x^i} \left[g^{1/2} \left(a_c^i + d_c^{ij} \frac{\partial f}{\partial x^j} \right) \right]$$

The components of a_c^i and d_c^{ij} can be obtained by transformation from expressions, e.g. in Ref. [19] of the collision operator written in local velocity coordinates (v, χ), $\chi = v/v_{||}$. The Jacobian of the transformation, $g^{1/2}$, can be shown to be independent of the angles, θ, the averaging of the collision operator is therefore simple

$$< C(f_0) > = g^{-1/2} \frac{\partial}{\partial I^i} \left[g^{1/2} \left(< a_c^{ij} > f_0 + < d_c^{ij} > \frac{\partial f_0}{\partial I^j} \right) \right]$$

The general form for the quasilinear operator has been derived by Kaufman [20] and its specialisation to ICRH is discussed in e.g. [15]. It has the form

$$< Q(f_0) > = g^{-1/2} \frac{\partial}{\partial I^i} \left[g^{1/2} D_{RF}^{ij} \frac{\partial f_0}{\partial I^j} \right]$$

The components of the tensor D_{RF}^{ij} will not be reproduced here. But they are all proportional to

$$D_{RF}^{ij} \sim \left| \sum_N \frac{Ze}{\omega \tau_b} \int_0^{\tau_b} \vec{v}_\perp \left[\vec{E}_+ J_{n+1}(k_\perp \rho) + \vec{E}_- J_{n-1}(k_\perp \rho) \right] e^{i\Phi(t)} dt \right|^2 , \qquad \frac{d\Phi}{dt} = n\omega_c - \omega + \vec{k} \cdot \vec{v}_g$$

where N is the toroidal mode number in a Fourier decomposition of the wave electric field, n gives the harmonic at which cyclotron interaction takes place, E_+ and E_- are the left- and right hand polarised components of the electric field, respectively, ρ is the Larmor radius and $\vec{v}_g$ is the guiding centre velocity.

As can be seen, both the collision and RF-operators can be written as divergencies in invariant space. The collision operator involves orbit averages of local collision coefficients, whereas the RF diffusion tensor is obtained by summing the "kicks" in energy an ion receives as it passes through cyclotron resonances along its orbit.

3.3 Monte Carlo Solution Of The Orbit Averaged Fokker-Plank Equation

The three dimensional Fokker-Plank equation can be solved by computer codes using finite element or finite difference methods. An alternative method is to use Monte Carlo techniques. The advantages with this method include: the central part of the computer program is in principle not very complicated and there are no particular problems with boundary

conditions. A short discussion of the Monte Carlo operators needed to solve the orbit averaged Fokker-Planck equation is given below.

When solving the orbit averaged Fokker-Planck equation with a Monte Carlo method, a large number of "particles" must be followed in invariant space. The invariants of a "particle at time step t_n are changed to those at the next time step ($t_{n+1} = t_n + \Delta t$) according to

$$I^i(t_{n+1}) = I^i(t_n) + \Delta I^i$$

The components of the Monte Carlo operator, ΔI^i, are stochastic variables, whose expectation values and convariances are

$$E\left[\Delta I^i\right] = \frac{d\mu^i}{dt}\Delta t, \qquad C\left[\Delta I^i, \Delta I^j\right] = \frac{d\sigma^{ij}}{dt}\Delta t$$

where the time drivatives of the expectation values, μ^i, and covariances, σ^{ij}, are obtained from the orbit averaged Fokker-Planck equation by following the time evolution a distribution function representing a single "particle" at $t = t_n$, $f_o\left(\vec{I}, t_n\right) = g^{-1/2}\delta\left(\vec{I} - \vec{I}_o\right)$,

$$\frac{d\mu^i}{dt} = \int I^i \frac{\partial f_0}{\partial t} g^{1/2} d^3I = < a_c^i > + g^{-1/2} \frac{\partial}{\partial I^j}\left[g^{1/2}\left(< d_c^{ij} > + D_{RF}^{ij}\right)\right]$$

$$\frac{d\sigma^{ij}}{dt} = \int \left(I^i - \mu^i\right)\left(I^j - \mu^i\right)\frac{\partial f_0}{\partial t} g^{1/2} d^3I = < d_c^{ij} + d_c^{ji} > + D_{RF}^{ij} + D_{RF}^{ji} = < 2d_c^{ij} > + 2D_{RF}^{ij}$$

The Monte Carlo operator can now be written as a sum of two components

$$\Delta I^i = \frac{d\mu^i}{dt}\Delta t + A^{ik}\xi^k\sqrt{\Delta t}$$

where ξ^k are uncorrelated stochastic variables with zero expectation values and unit variances; the matrix A^{ik} must fulfil relation: $A^{ik}\,A^{jk} = d\sigma^{ij}/dt$. How to solve the equation for A^{ij} is outlined in Refs. [15,21].

The procedure to follow in a computer program using the above Monte Carlo operator is the following: calculate the orbit averaged collision coefficients and the RF-diffusion tensor; evaluate the two components of the Monte Carlo operator and store them on a grid in invariant space; load the "particles" with a Maxwellian distribution; advance a time step Δt by applying the Monte Carlo operator, which is found by interpolation in the pre-calculated table, to each particle; repeat until the end of the calculation. A Monte Carlo code named FIDO working

along these lines have been developed. For further information about the FIDO code see Ref. [22].

3.4 Numerical results from the FIDO code

In this paragraph results from the newly developed FIDO code are compared with those of the simplified model in PION-TO. The aim being to assess the applicability of the simplified modelling for predicting measured quantities like the fast ion energy content.

The following test case has been used in the simulations: Hydrogen minority heating in a deuterium plasma, JET sized plasma with a constant current profile (to facilitate the comparison between the codes) and a total current of 2 MA, $n_H/(n_H + n_D) = 6\%$, $n_D = 3.10^{19}$ m^{-3} $(1 - 0.9\ s^2)^{1/2}$, $T_e = T_D = 8$ keV $(1 - s^2)^2$, $B_o = 2.8$ T, f = 42.7 MHz, the profile of left hand component of the wave electric field has been assumed to the proportional to $E_+ \sim \exp(- s/0.25)^2)$ and the right hand component E_- has been set to zero. Thus, in the PION-TO calculations the power deposition has been replaced with the above model for E_+.

Fig. 7 shows the volume integrated flux surface averaged hydrogen energy density profile

$$W_H(s) = \int_o^s w_H(s) \frac{dV}{ds} ds$$

calculated for 6 MW of absorbed RF power.

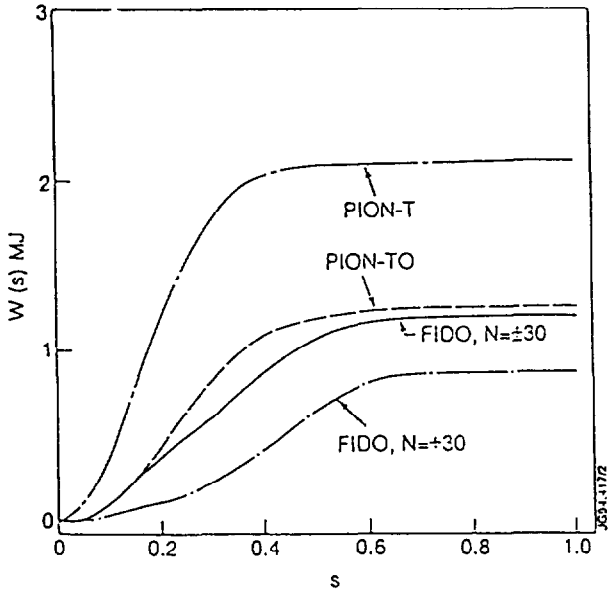

Fig. 7 Volume integrated flux surface averaged energy density of the hydrogen ions.

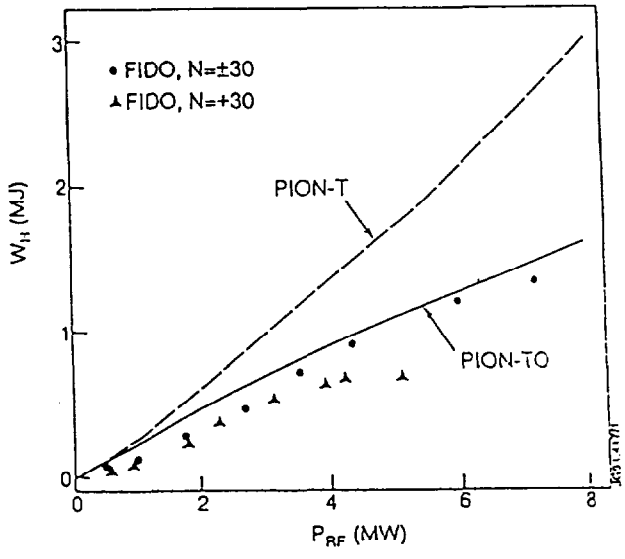

Fig. 8 Total energy content of the hydrogen ions.

The FIDO simulations has been carried out for two different toroidal mode number spectra of the wave field. One with N = ± 30, which is representative of dipole phasing of the JET antennas, and one with an asymmetric spectrum of N = + 30. Asymmetric spectra are of importance for current drive applications, e.g. minority current drive. Here N = + 30 has been used to clearly demonstrate the effect of an asymmetric spectrum. In addition to curves from FIDO, profiles calculated with PION-TO and PION-T (i.e. the zero banana width version) are also shown in Fig. 7. As can be seen, the profile is much more peaked and the total energy content significantly higher in the zero banana width calculation than in those where the finite orbit width has been included. The profile from PION-TO is slightly narrower than that of FIDO for N = ± 30, as expected. In line with the findings in Ref. [8], the dominant process leading to transport of the fast particles is here a neoclassical effect caused by the slowing down of the fast ions on the electrons. There is a quite significant difference between N = ± 30 and N = + 30. The total energy content is lower and the profile is broader for N = + 30. This is caused by a substantial RF-induced drift of the fast particles for N = + 30, pushing them out of the region with high wave field. Since there are less absorbing ions in the centre one has to incease the wave field strength to achieve the same power.

In Fig. 8 the total energy content of the hydrogen ions has been plotted as a function of the absorbed RF-power. For high powers the zero banana width calculations, PION-T, gives energy contents substantially above those which includes finite orbit width effects. The results from PION-TO are somewhat, but not significantly, higher than those from FIDO with N = ± 30. In the case of N = + 30 the resonating ions are increasingly driven out from the centre as the power increases giving rise to lower energy contents at high power.

From these examples it is clear that finite orbit width effects play an important role. Furthermore, the simplified modelling in PION-TO yields, for symmetric antenna spectra, results which are in reasonable agreement with the more complete FIDO calculations. Simulations with codes like FIDO are necessary for detailed studies and, in particular, for asymmetric antenna spectra. For further applications of the FIDO code see Ref. [23].

4. CONCLUSIONS

The PION-T code has been used to simulate experimental results for a number of JET discharges. At low characteristic power densities good agreement can be obtained, giving support for classical slowing down and the peaked power deposition profiles calculated by wave propagation codes. However, at high characteristic power densities discrepancies appear. These discrepancies seem to be caused by finite orbit width effects. When such effects are included, in a simplified way, in the PION-TO code good agreement can be obtained also at higher power densities.

Finite orbit width effects can be treated more rigorously with a three dimensional orbit averaged Fokker-Planck equation. To take these effects into account a code called FIDO